Mechanical Characterization of Low-Carbon Steels for High-Field Accelerator Magnets: Application to Nb_3Sn Low-β Quadrupole MQXF

I. Aviles Santillana, G. Vallone, E. Anderssen, S. Izquierdo Bermudez, S. Bonnin, M. D. Crouvizier, R. Principe, S. Sgobba, K. P. Weiss, N. Bagrets, C. J. Huang, and L. F. Li

***Abstract*—In the quest for higher field accelerator superconducting magnets, essential parts of their design are the so called yokes, which are traditionally made of low – carbon magnetic steel. In currently used magnets, they are typically found in the form of fine – blanked laminations, or machined from laminated heavy plates. The material's choice is made based on a compromise between the high saturation field, providing a return path for the magnetic flux, and the mechanical robustness conferred to the magnets' cold masses. This paper describes the mechanical characterization of low – carbon steel, and applies several approaches for the design and validation of the material from the structural point of view, applicable to a Nb_3Sn quadrupole: MQXF. Tensile tests at room and cryogenic temperatures, together with fatigue and fracture toughness at cryogenic temperature have been performed. Calculations based on the obtained material properties and results of extensive non-destructive examination (ultrasonic testing) have been implemented in order to ascertain the structural limits of low – carbon steel for its use in the fabrication of high field accelerator superconducting magnets.**

***Index Terms*—Cryogenic testing, high field superconducting magnets, low carbon steel, mechanical characterization.**

I. Introduction

THE first large accelerator with superconducting magnets was built at the Fermi National Accelerator Laboratory (FNAL). The successful dipole and quadrupole magnets developed at FNAL have strongly influenced later designs of superconducting accelerator magnets such as the Hadron-Electron Ring Accelerator (HERA) or the Large Hadron Collider (LHC) [1], [2]. It has come a long way since the Tevatron, but even the latest designs of future accelerators such as the Future Circular Collider (FCC) [3] have a common element that has endured over time: the iron yoke.

The yoke, in early versions of superconducting magnets, was just a hollow cylinder mounted concentrically around the coil [1], [2], but the hollow cylinder has given way to more complex and optimized geometries, which are always found around the coils. Magnetically, it serves three purposes: increase the magnet's field, shields the surroundings against stray fields by closing the magnetic circuit, and reduce the stored magnetic energy [1], [2]. Additionally, it can have a key mechanical function, providing structural integrity and mechanical stability to the magnet's body.

In this paper, we present the results of a comprehensive mechanical characterization of extra low - carbon steel, including at cryogenic temperature, and a systematic ultrasonic volumetric examination of some of components after final machining. These results are used in a Finite Element Model (FEM) in order to perform a detailed mechanical assessment applicable to low-β Nb_3Sn quadrupoles.

I. Aviles Santillana, S. Izquierdo Bermudez, S. Bonnin, M. D. Crouvizier, R. Principe, and S. Sgobba are with European Organization for Nuclear Research (CERN), 1208 Geneva, Switzerland (e-mail: iaviles@cern.ch).

G. Vallone and E. Anderssen are with Lawrence Berkeley National Laboratory, Berkeley, CA 94720 USA.

K. P. Weiss and N. Bagrets are with the Institute for Technical Physics, KIT, 76344 Eggenstein-Leopoldshafen, Germany.

C. J. Huang and L. F. Li are with the Technical Institute of Physics and Chemistry, Chinese Academy of Sciences, Beijing 100190, China.

Color versions of one or more figures in this article are available at https://doi.org/10.1109/TASC.2022.3149853.

II. The MQXF Magnet

The main objective of the High Luminosity (HiLumi) Large Hadron Collider (LHC) project is to develop a set of beam parameters and the hardware configuration that will enable the LHC to reach an integrated luminosity of 250 fb^{-1} per year, enabling the goal of 3000 fb^{-1} twelve years after the upgrade. This luminosity is about ten times the luminosity reach of the first twelve years of the LHC lifetime [4]. In order to reach this unprecedented integrated luminosity, major upgrades need to be done at the interaction regions. Amongst them, the installation of newly developed low-β Nb_3Sn quadrupoles, called MQXF [5], [6].

The MQXF quadrupole magnets will provide a nominal gradient of 132.6 T/m, in a 150 mm large aperture, with a conductor peak field of 11.4 T [5]. They are being developed in the framework of a collaboration between the CERN HL-LHC project and the US-LARP (LHC Accelerator Research Program) in a two - step approach: fabrication assembly and test of the short models (MQXFS), followed by the accelerator magnets (MQXFA: 4.2 m magnetic length, and MQXFB: 7.15 m magnetic length). Both short models and accelerator magnets share the same cross-section [5], shown in ??. The performance of the design was successfully tested with short models (1.2 m magnetic length) [7]–[10].

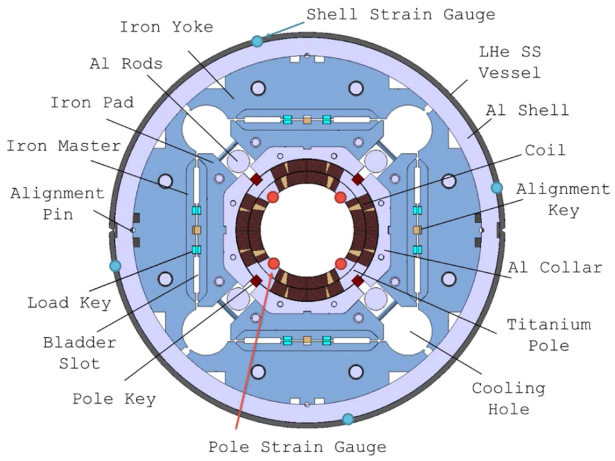

Fig. 1. Cross section of the MQXF magnet, with the description of the various components. The yoke and pads are made of 5.6 mm thick laminations, while each iron master is made of a single solid piece for the short model MQXFS series, and two pieces for the longer MQXFA and MQXFB series.

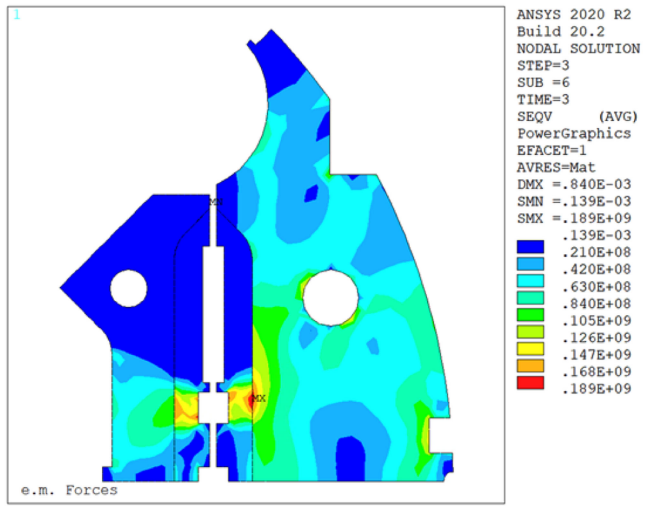

Fig. 2. Von Mises stress distribution in the iron yoke at room temperature when the stress applied to the coil (prestress on the winding pole) is 145 MPa.

A. *Mechanical Design*

The MQXF cross-section is shown in Fig. 1: the superconducting coils are held by laminated aluminium collars and iron pads. Solid masters allow for the insertion of load keys and water pressurized bladders between the pads and the iron yoke. An aluminium shell and a stainless steel vessel close the mechanical structure. The bladders allow to stretch the aluminium shell and compress the superconducting coils at room temperature. Load keys are then inserted to lock the magnet in this prestressed state [11]. The prestress is then increased during the cooldown to cryogenic temperatures by the differential thermal contraction of the various components. The applied coil compression attempts to avoid the potential detachment of the superconducting coil from the winding pole during powering [12]. The behaviour of this critical interface was measured on short models and early prototypes with strain gauges, installed on the winding pole (see Fig. 1). Measurements showed that an azimuthal prestress of $145\,\mathrm{MPa}$ on the winding pole is required to completely avoid pole/coil unloading and interfacial debonding during powering [13].

III. Mechanical Testing Program and Non - Destructive Examination

A comprehensive mechanical characterization test program was conceived in order to assess the mechanical properties of extra - low carbon steel both at room temperature and close - to - service temperature (4 K). The test campaign comprises quasi-static testing (tensile tests), cyclic testing (fatigue tests) and fracture mechanics of as received (after hot rolling) as a reference and annealed (980 °C, 1 h) material. It was produced by the company Thyssenkrupp under the trademark name ARMCO grade 4, with a maximum of 10 ppm of carbon, in the form of 5.6 mm thick fine - blanked laminations. Additionally, a volumetric non - destructive examination test campaign (ultrasonic testing (UT)) was performed in order to validate the whole production of finished pieces of masters, which are 3.7 m (half the magnets' length) long components, machined from thick (20 mm) ARMCO plates. Imperfections were identified and their size was accurately determined.

TABLE I
Results of Mechanical Testing At Room Temperature

Material	R_{eL} [MPa]	R_m [MPa]	A [%]
As received. Rolling direction	229 ± 1	293 ± 2	42 ± 1
Annealed. Rolling direction	237 ± 3	304 ± 2	41 ± 2
Annealed. Transverse direction	251 ± 1	301 ± 1	44 ± 2

A. *Tensile Tests*

Uni-axial tensile tests were performed according to ISO 6892-1 at room temperature on standard size specimens of 4 mm thickness. Three specimens of each type were tested. The results to be considered are the tensile strength R_m and the lower yield strength R_{eL}. The first shall be below $290\,\mathrm{MPa}$ to avoid excessive production costs in the case of fine blanked laminations [14], whereas the latter shall be above 190 MPa, the maximum Von Mises stress at the iron yoke at room temperature (see Fig. 2), when the azimuthal prestress applied to the coil reaches $145\,\mathrm{MPa}$ for the case studied of this paper: the MQXF magnet [13]. This is to avoid any eventual unloading of the magnet at ultimate current.

295 K results are shown in Table I. The lower yield strength largely exceeds the required minimum value of 145 MPa, whereas the tensile strength would be slightly higher than ideally desired in order to optimize the fabrication costs, specially if a big production is envisaged [15]. Tensile properties at room temperature after annealing are practically equivalent to the as hot - rolled state. In the annealed condition, there is an subtle increase of R_{eL} in transverse direction with respect to the longitudinal (rolling) direction.

Additionally, tensile tests in liquid helium have been performed at CERN, according to ISO 6892-4. Due to the inherent brittleness of the material at cryogenic temperature, the width at the calibrated length was reduced with respect to the standard dimensions in order to guarantee that the failure occurs at the region covered by the extensometers, far from the heads. The setup of the cryogenic tensile tests is shown in Fig. 3.

The results are gathered in Table II, where it can be seen that there is a substantial increase in tensile strength with respect to room temperature values. This fact is accompanied by a drastic decrease in ductility, with all specimen fail in the

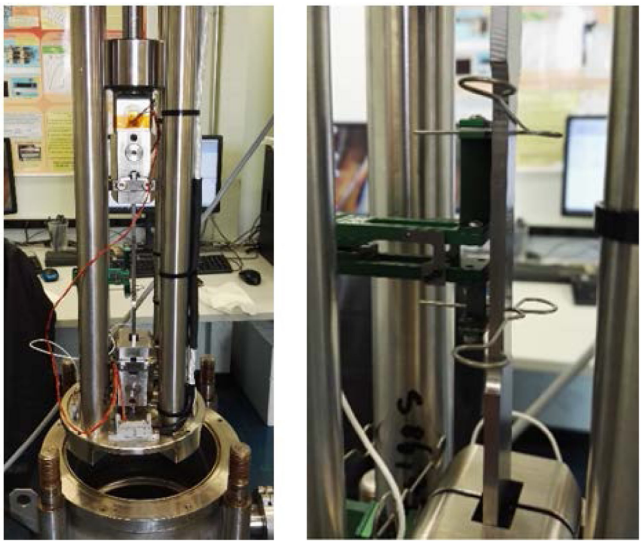

Fig. 3. Setup of cryogenic tensile test, showing the specimen mounted in the cryostat (left), and a closeup of the extensometer coupled to it (right).

TABLE II
RESULTS OF TENSILE TESTING AT CRYOGENIC TEMPERATURE (4 K)

Material	R_m [MPa]	A [%]
As received. Rolling direction	1034 ± 4	0.4 ± 0.1
Annealed. Rolling direction	972 ± 8	0.2 ± 0.1
Annealed. Transverse direction	975 ± 6	0.3 ± 0.1

elastic region, denoting an evident brittleness. Results show a very limited spread between specimens. Practically identical mechanical properties are measured in the two directions tested after annealing. A marginal decrease of tensile strength at cryogenic temperature (less than 10%) is observed after annealing treatment.

B. Fatigue Tests

As it is widely know, the LHC is not a pulsed machine. However, in order to restrain the repulsive Lorentz forces during powering and unpowering of the superconducting coils, during its whole lifespan, it can be considered that the yoke is submitted to cyclic efforts. Taking this into account, and in order to rule out a premature failure of the components, fatigue tests were performed at the Center of Cryogenic Materials and Applied Superconductivity in Beijing (CN).

Fatigue tests in force control mode were performed on standard hourglass specimens of 4 mm thickness according to ASTM E466. Test parameters were tailored for the MQXF case. In order to account for an effective alternating stress of 300 MPa and a stress ratio R = 0.1, the Goodman formula was used, resulting in a maximum stress off 500 MPa. The frequency was kept sufficiently low (7 Hz) to avoid an excessive temperature rise of the sample based on the studies of Ogata *et al.* [16]. For the requirements in terms of number of cycles, a CERN specification was used [17], which considers a continuous LHC operation during 20 years, 250 days of operation per year and 4 ramps per day, applying an extra margin, is 20000. A factor of 20 to the number of cycles is then applied, based on the ITER magnet system technical specification [18], resulting in the requirement of 400000 cycles without failure.

Three specimens of each type (i.e. as received LD, annealed LD and annealed TD) were tested. The outcome of the cryogenic fatigue testing campaign is that every single specimen survived the required number of cycles.

TABLE III
RESULTS OF FRACTURE TOUGHNESS AT CRYOGENIC TEMPERATURE (4 K)

Material	K_{IC} [MPa$\sqrt{\text{m}}$]
As received. (L-T)$_1$	27.98 ± 0.22
As received. (L-T)$_2$	26.91 ± 0.22
Annealed. (L-T)$_1$	25.37 ± 0.21
Annealed. (L-T)$_2$	28.17 ± 0.53
Annealed. (T-L)$_1$	24.44 ± 0.16
Annealed. (T-L)$_2$	25.71 ± 0.52

C. Fracture Toughness Tests

Size - independent plain - strain fracture toughness is an essential material property if a damage tolerant approach to design is implemented. Based on the results of tensile tests at 4 K shown in Table II and material properties gathered from literature for a very similar material [14], ARMCO is expected to fail in the elastic domain. Thus, Linear-Elastic Plain-Strain Fracture Mechanics test according to ASTM E399 at cryogenic temperature (4 K) were performed at the Cryogenic Material Test Lab Karlsruhe (CryoMaK), at the Institute for Technical Physics in Karlsruhe (DE).

Two 5.8 mm thickness compact tension specimens of each type were tested. Similarly to the tensile and fatigue tests, only one direction was tested for the as - received state (L-T), for reference, whereas two perpendicular directions (L-T and T-L) were tested for the annealed material. As it is described in ASTM E399, the first letter of the two-letter code designates the direction normal to the crack plane, and the second letter, the expected direction of crack propagation.

The results of fracture toughness tests are gathered in Table III. It can be seen that for equivalent specimens, the spread is very limited. Material exhibits similar fracture toughness in L-T and T-L directions. Annealing HT induced had practically no effect on fracture toughness at cryogenic temperature.

D. Ultrasonic Testing

Ultrasonic examination (UT) was performed in the 62 masters which will be used for the fabrication of the MQXF long magnets (MQXFA and MQXFB) at CERN. These masters are long slender pieces, with approximate dimensions 3760 mm $\times$ 226 mm $\times$ 15 mm (see Fig. 4). They were ultrasonically inspected after machining to their final geometry ($R_a < 6.3\,\mu m$) from laminated ARMCO grade 4 heavy plates.

UT inspection was performed according to EN 10160: Ultrasonic examination of steel flat product of thickness equal or greater than 6 mm (reflection method). The same standard was used for the acceptance criteria. In order to control 100% of the volume, the inspection was performed, using longitudinal waves, in two times: first, 90% of the volume was inspected via Phased Array Ultrasonic Testing (PAUT). Additionally, for the regions not accessible by PAUT, conventional UT was applied. PAUT by contact was performed with a 5 MHz, 32 element dual array probe (1.5 mm pitch, 4.75 mm elevation). Conventional

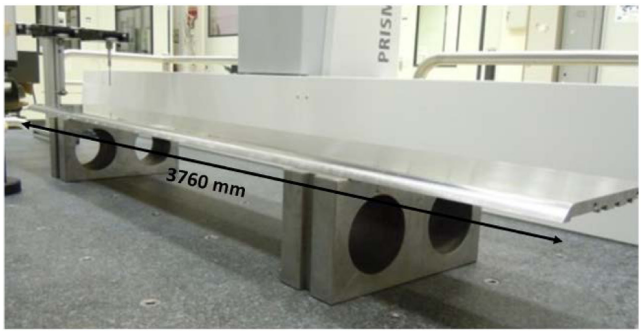

Fig. 4. Iron master during dimensional metrology measurement, giving an idea of the slenderness of the piece. Its cross section can be seen on the right of the image. The longitudinal dimension is indicated.

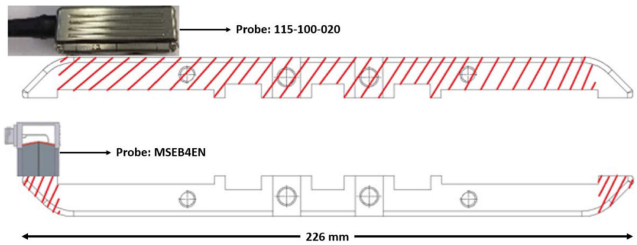

Fig. 5. Sketch of the two steps of UT examination, depicting a cross section of the piece together with the probe which is used. The red - stripped region is the volume that is covered with PAUT (top) and conventional UT (bottom)(left). The positions of the probes with respect to the piece are representative of the UT inspection, but the size of the probes is exaggerated for clarity.

UT was performed with a ϕ 10 mm, 4 MHz dual element probe. A sketch of the UT examination, showing the volumes covered (10152 cm^3 per piece) at each step and the position of the probes at each of them is shown in Fig. 5.

In order to quantify the size of the imperfections that could eventually be found in the pieces, a dedicated reference block was machined from spare material of the same production, thus fully representative. Flat - bottomed holes (FBH) of ϕ 3 mm and ϕ 5 mm where machined at different depths were introduced in this block, used for the sensitivity calibration curves: Time Correction Gain (TCG) for PAUT and Distance Amplitude Correction (DAC) for conventional UT.

From the 96 pieces which were inspected, no indications larger than equivalent FBH ϕ 1.2 mm were detected in 92 pieces which are considered as acceptable based on the experimentally measured fracture toughness at 4 K and the maximum stress value calculated for the iron yoke. This figure will serve as maximum flaw size which is actually present in the yoke. Four masters showed indications between FBH 1.2 mm and FBH 5.0 mm reflectivity,thus being considered unacceptable and being discarded for the production.

To be noted that, for practical reasons, the hundreds of rolled parts were not inspected via UT examination. Since they come from the same production, which was just rolled further to achieve a thinner product, they are expected to have a maximum flaw size lower to the one detected in the masters due to the higher reduction implemented. Nevertheless, a statistical quality control via UT of these elements is highly desirable to ensure conformance, and should be enforced for future productions.

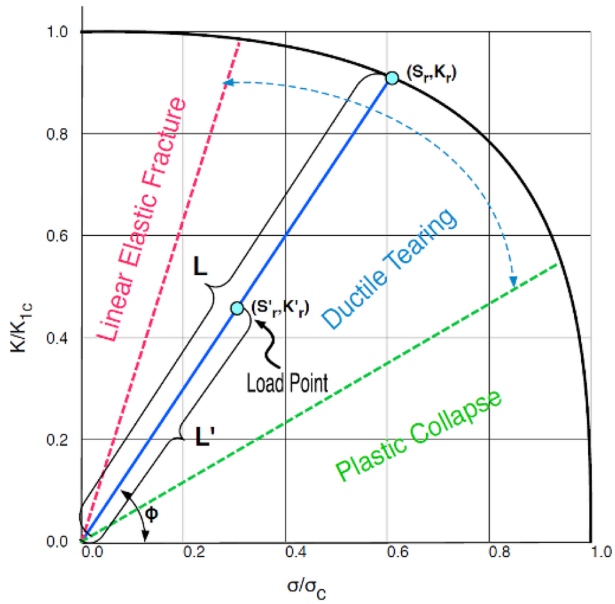

Fig. 6. The failure assessment diagram, as suggested in the R6 methodology.

IV. Failure Assessment of Iron Structures

The MQXF magnet allows to control the prestress by varying the thickness of the loading keys. The increase of prestress results in an increase of the load on the various components. As a consequence, the maximum prestress that can be applied to the magnet is limited by the stresses produced on those components, and their material properties. Here we use the material limits measured in the previous sections to establish practical limits on the loads applied to the MQXF magnet. The results use 3D magneto-mechanical models of the magnet, created in Opera and ANSYS APDL. A detailed discussion of the model assumptions, results, and a comparison with the experimental measurements can be found in [19]–[21].

A. Failure Assessment Diagram Verification

The verification of the iron components is performed using an R6 analysis with a Failure Assessment Diagram (FAD). The procedure and assumptions of such analysis are described in [22]. The same methodology was already used on the MQXF magnet to study the failure of an aluminum shell and to refine its design [23], [24]. A typical FAD diagram is shown in Fig. 6.

The limit failure curve can be computed as follows:

$$K_r(S_r) = S_r \left[\frac{8}{\pi^2} \log \left(\sec \left(\frac{\pi}{2} S_r \right) \right) \right]^{-1/2} \tag{1}$$

where K_r and S_r are adimensional parameters, functions of the material strength σ_c and toughness K_{Ic}:

$$S_r = \frac{\sigma}{\sigma_c} \qquad K_r = \frac{K}{K_{Ic}} \tag{2}$$

For the MQXF iron components, the strength and fracture toughness at 4 K are equal to 974 MPa, and 26 MPa$\sqrt{\text{m}}$ respectively (see Tables II and III). The points inside the failure curve are considered safe, and the load factor η can be computed by

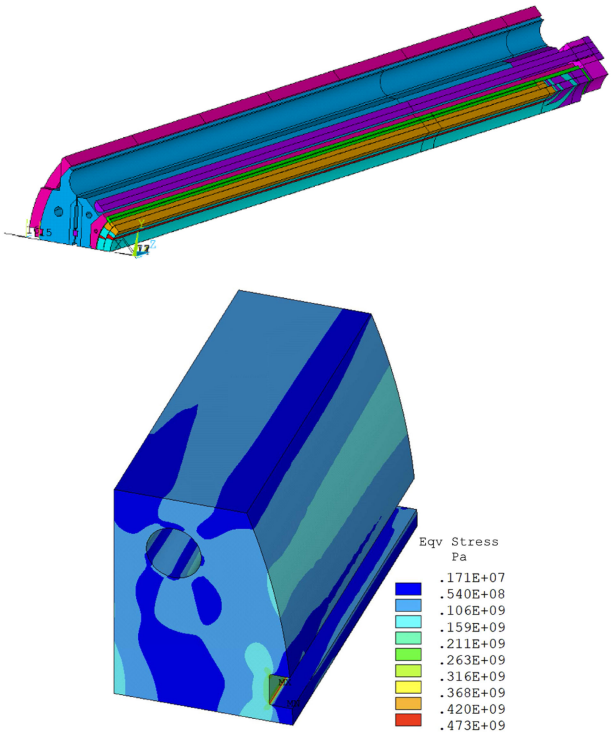

Fig. 7. Finite element models of the MQXF magnet: global model (top) and yoke submodel with the equivalent stress contours (bottom).

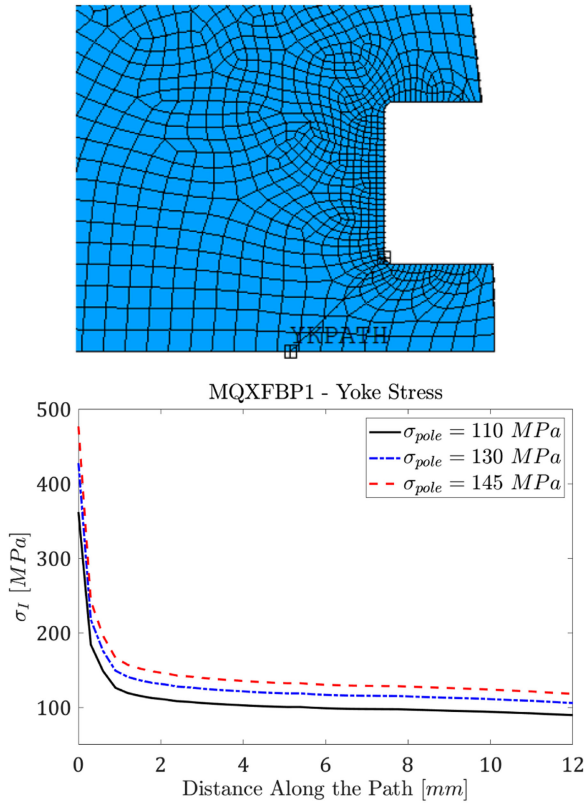

Fig. 8. View of the path used to extract the applied stresses on the submodel (top), and computed stresses as a function of the path position (bottom).

projecting the loading point onto the curve:

$$\eta = \sqrt{\frac{(S_r^2 + K_r^2)}{(S_r'^2 + K_r'^2)}} \tag{3}$$

In a linear model, multiplying the applied loads for this factor would bring the loading point on the failure curve.

B. Load Limits of the MQXF Iron Yoke

A two-step FE analysis was performed in order to compute the stresses in the iron components: first, a global model (Fig. 7, top) was used to identify the critical regions of the yoke. Then, a refined FE submodel only of the most critical region was created (Fig. 7, bottom). The displacements from the global model were extracted and applied on the cut-boundary of the submodel. The global model was run considering a prestress of 145 MPa on the winding pole. As underlined previously, this is the value required to avoid unloading at any stage of the magnet powering. In practical terms, this means that the magnet design would never require a higher value of prestress.

The stress was extracted on a path going from the peak stress location, along the minimum gradient line, as shown in Fig. 8. The stress profile on the critical path is largely independent from the particular magnet studied, as very similar numbers are obtained when running different length magnets, as for example the short models MQXFS or the MQXFB magnets. The peak stress is equal to 475 MPa, and quickly decreases within about 1 mm to less than 200 MPa. Weight functions were used to extract the expected K_I as a function of the crack length and width. The load factor η was computed using (3). Results are shown in Fig. 9 as a function of the crack length $2a$ and width $2c$. It is interesting to notice that, for certain crack widths, the load

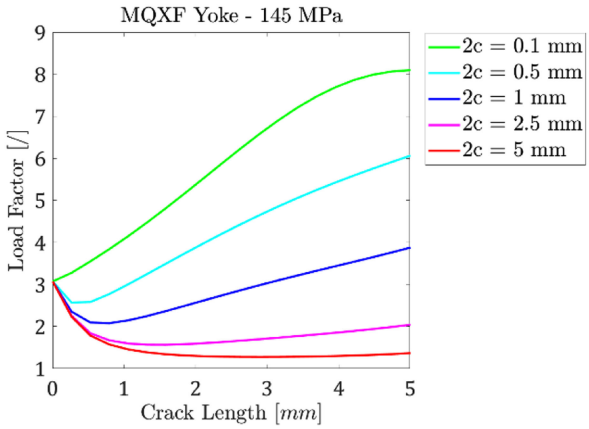

Fig. 9. Load factor for the MQXF yoke as a function of the crack length and width.

factor can increase with the crack length: this is a consequence of the fact that for the considered stress profile K_I increases but the stress at the crack tip decreases. A reasonable crack size detection threshold, assuming a UT inspection with a flat bottom hole FBH, would be 1.2 mm, as it was shown in subsection D. Ultrasonic testing. For this crack size, and assuming $a = c$, we get a very safe load factor of 2.

The position on the FAD diagram as a function of the crack length is provided in Fig. 10. The plot shows that, as the crack length increases, the stress intensity ratio decreases and the expected failure mode moves from plastic collapse to linear elastic fracture.

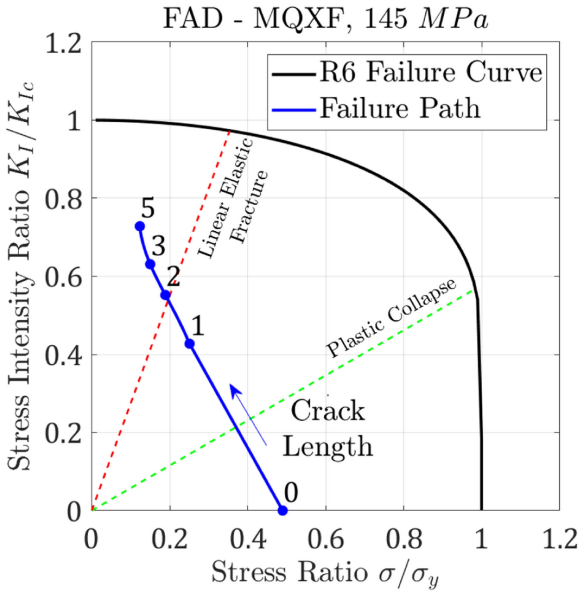

Fig. 10. FAD results for the MQXF magnet, as a function of the crack length (in mm), and assuming $a = c$.

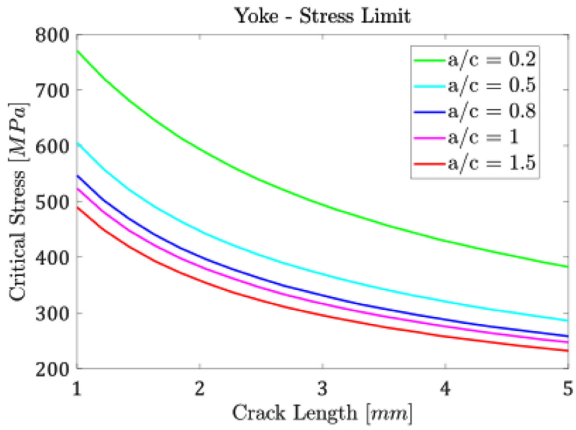

Fig. 11. Stress limits for the material as a function of the crack size.

TABLE IV
CRITICAL STRESS AT 4 K COMPUTED WITH THE SIMPLIFIED APPROACH FOR DIFFERENT FBHS CORRESPONDING TO UT TESTING CLASS FROM EN 4050-4

Class	FBH [mm]	Critical stress (σ_c) $[MPa]$	$\sigma_c(FoS = 1.2)$ $[MPa]$
7	0.6	645	538
6	0.8	575	479
5	1.2	483	403
4	1.6	424	353
3	2.0	382	318
2	3.2	306	255
1	5.0	247	206

V. SIMPLIFIED APPROACH

Designing a magnet can require the evaluation of the performances of many different coil and structure designs. The process of assuming a crack position and then estimating the crack propagation could significantly affect the time required to evaluate the feasibility of any magnet design. As a consequence, here we propose a simplified and very conservative approach that would allow to compute a limit on the basis of the average stress.

In general, one can assume that a crack might be present in any location of the body. If the loads are generated by relative deformations (e.g. because of differential thermal contractions), and applied in a quasi-static fashion, it is possible to assume that the crack will propagate until it becomes circular (penny shaped). After this propagation, the crack will have as characteristic dimension the largest one detected during scanning. As the crack can be anywhere in the body, the stress profile along its length can change significantly. We can conservatively assume that the stress will be equal to the maximum value, computed with numerical or analytical models (constant), along the whole crack path. The selection of the weight function has to consider either an edge crack or a crack embedded in the body. The result of these assumptions is that, for a given applied stress and crack size, it is possible to immediately compute a conservative position on the FAD diagram. Fixing the maximum allowed crack size to be allowed after inspection, it is possible to obtain a maximum allowed (critical) stress for preliminary design operations. On the other hand, this would also mean that, when a higher stress is required, a more detailed inspection can be performed, increasing the material limits.

The results for the considered low-carbon steel are reported in Fig. 11, which shows the critical stress as a function of the crack length and crack width. The critical stress is the one that brings the load point on the FAD critical line (load factor equal to 1). On top of this, the designer has always to consider an appropriate factor of safety (FoS). Because of the non-linear nature of the weight functions, the factor of safety will be linear only in the stress but not in the crack length. Assuming a FoS of 1.2, and a crack size of 1.2 mm (based on UT results), the critical stress at 4.5 K for the considered steel is equal to 403 MPa.

In addition to this result, by using this simplified approach, we can calculate the critical stress for different crack sizes, which in these case are associated to FBHs and the corresponding class for UT inspection from EN 4050-4 [25] (see Table IV. This means that, by defining the acceptance class of UT inspection, the critical stress is automatically defined.

The strong assumptions of this section allow to obtain material limits that can be used in everyday design operations. However, in certain areas of the iron components these stress limits might still be exceeded. Since the previous approach is very conservative, this would not imply that that area would really experience a mechanical failure. It is possible then to verify most dangerous area, when necessary, with the refined approach proposed in Section IV-A.

VI. CONCLUSION

A comprehensive mechanical characterization of low carbon steel has been performed both at room temperature and at cryogenic temperature (4 K), including tensile, fatigue and fracture toughness tests. These results, in combination with the extensive ultrasonic examination performed, gives a solid experimental basis for a detailed failure assessment of the yoke of high - field accelerator magnets.

FAD analysis was performed on the MQXF magnet yoke. For the maximum design prestress and a crack smaller than 1.2 mm, the computed load factor is larger than 2. A simplified approach is proposed to compute the maximum allowed stress as a function of the inspection criteria. With a maximum crack size of 1.2 mm, a stress of 403 MPa at 4.5 K allows a safety factor larger than 1.2. Both methodologies are general and henceforth their usage is not limited to the MQXF magnet.

REFERENCES

[1] K.-H. Mess *et al.*, *Superconducting Accelerator Magnets*. World Scientific, 1996.

[2] L. Rossi and L. Bottura, "Superconducting magnets for particle accelerators," *Rev. Accel. Sci. Technol.*, vol. 5, pp. 51–89, 2012.

[3] D. Schoerling *et al.*, "The 16 T dipole development program for FCC and HE-LHC," *IEEE Trans. Appl. Supercond.*, vol. 29, no. 5, Aug. 2019, Art. no. 4003109.

[4] L. Rossi and O. Brüning, "High luminosity large hadron collider: A description for the European strategy preparatory group," Geneva, Swtizerland: CERN, 2012.

[5] P. Ferracin *et al.*, "Development of MQXF: The Nb_3Sn low-β quadrupole for the HiLumi LHC," *IEEE Trans. Appl. Supercond.*, vol. 26, no. 4, Jun. 2016, Art. no. 4000207.

[6] E. Todesco *et al.*, "Design studies for the low-beta quadrupoles for the LHC luminosity upgrade," *IEEE Trans. Appl. Supercond.*, vol. 23, no. 3, Jun. 2013, Art. no. 4002405.

[7] G. Chlachidze *et al.*, "Performance of the first short model 150-mm-aperture quadrupole MQXFS for the high-luminosity LHC upgrade," *IEEE Trans. Appl. Supercond.*, vol. 27, no. 4, Jun. 2017, Art. no. 4000205.

[8] H. Bajas *et al.*, "Test result of the short models MQXFS3 and MQXFS5 for the HL-LHC upgrade," *IEEE Trans. Appl. Supercond.*, vol. 28, no. 3, Apr. 2018, Art. no. 4007006.

[9] S. Stoynev *et al.*, "Summary of test results of MQXFS1–The first short model 150 mm aperture quadrupole for the high-luminosity LHC upgrade," *IEEE Trans. Appl. Supercond.*, vol. 28, no. 3, Apr. 2018, Art. no. 4001705.

[10] F. Mangiarotti *et al.*, "Test results of the CERN HL-LHC low-β quadrupole short models MQXFS3c and MQXFS4," *IEEE Trans. Appl. Supercond.*, vol. 29, no. 5, Aug. 2019, Art. no. 4001705.

[11] S. Caspi *et al.*, "The use of pressurized bladders for stress control of superconducting magnets," *IEEE Trans. Appl. Supercond.*, vol. 11, no. 1, pp. 2272–2275, Mar. 2001.

[12] G. Vallone and P. Ferracin, "Modeling coil-pole debonding in Nb_3Sn superconducting magnets for particle accelerators," *IEEE Trans. Appl. Supercond.*, vol. 27, no. 8, Dec. 2017, Art. no. 4004611.

[13] G. Vallone *et al.*, "Mechanical analysis of the short model magnets for the Nb_3Sn low-β quadrupole MQXF," *IEEE Trans. Appl. Supercond.*, vol. 28, no. 3, Apr. 2018, Art. no. 4003106.

[14] F. Bertinelli, S. Comel, P. Harlet, G. Peiro, A. Russo, and A. Taquet, "Production of low-carbon magnetic steel for the LHC superconducting dipole and quadrupole magnets," *IEEE Trans. Appl. Supercond.*, vol. 16, no. 2, pp. 1777–1781, Jun. 2006.

[15] M. Benedikt and F. Zimmermann, "Future circular colliders," *Proc. Int. Sch. Phys. Fermi*, vol. 194, pp. 73–80, 2016.

[16] T. Ogata, T. Yuri, and Y. Ono, "Review of specimen heating in mechanical tests at cryogenic temperatures," in *Proc. AIP Conf. Proc.*, 2014, vol. 1574, pp. 86–91.

[17] P. Fessia, "Specification for the consolidation of the LHC 13-kA interconnections in the continuous cryostat," *CERN EDMS Reference 1171853*, 2011.

[18] "Design description document: Magnets, section 1: Engineering description," *ITER IDM Reference 22HV5L, Version 2.2*, 2007.

[19] G. Vallone *et al.*, "Mechanical performance of short models for MQXF, the Nb_3Sn low-β quadrupole for the Hi-Lumi LHC," *IEEE Trans. Appl. Supercond.*, vol. 27, no. 4, Jun. 2017, Art. no. 4002906.

[20] G. Vallone *et al.*, "Mechanical performance of short models for MQXF, the Nb_3Sn low-β quadrupole for the Hi-Lumi LHC," *IEEE Trans. Appl. Supercond.*, vol. 27, no. 4, Jun. 2017, Art. no. 4002906.

[21] G. Vallone *et al.*, "Summary of the mechanical performances of the 1.5 m long models of the Nb_3Sn low-β quadrupole MQXF," *IEEE Trans. Appl. Supercond.*, vol. 29, no. 5, Aug. 2019, Art. no. 4002805.

[22] I. Milne, R. A. Ainsworth, A. R. Dowling, and A. T. Stewart, "Assessment of the integrity of structures containing defects," *Int. J. Pressure Vessels Piping*, vol. 32, no. 1, pp. 3–104, 1988.

[23] H. Pan, E. C. Anderssen, D. W. Cheng, S. O. Prestemon, and G. Ambrosio, "Failure assessments for MQXF magnet support structure with a graded approach," *IEEE Trans. Appl. Supercond.*, vol. 29, no. 5, Aug. 2019, Art. no. 8401507.

[24] H. Pan *et al.*, "Fracture failure analysis for MQXFA magnet aluminum shells," *IEEE Trans. Appl. Supercond.*, vol. 30, no. 4, Jun. 2020, Art. no. 4002307.

[25] BS EN 4050-4:2012, "Test method for metallic materials. Ultrasonic inspection of bars, plates, forging stock and forgings. Acceptance criteria," *Aerosp. Ser.*, 2012.